FULL PAPER

Calculating the Universal Energy-Level Alignment of Organic Molecules on Metal Oxides

Lothar Ley, Yaou Smets, Christopher I. Pakes, and Jürgen Ristein**

Recently, Greiner et al. [*Nat. Mater.* 2012, *11*, *76*] published a survey of the level alignment of about 40 metal oxide/organic molecule interfaces. They observed a striking regularity in the electronic level alignment of the highest occupied molecular orbital (HOMO) and the Fermi level that depends solely on the difference between the substrate work function and the ionization energy of the molecule independent of the details of the electronic structure of the oxide. The authors could reproduce their data under the assumption of thermodynamic equilibrium occupation of the HOMO using four adjustable parameters. A model that quantifies well-established concepts in heterojunction physics and achieves the same result without any adjustable parameters is presented here. This approach explains why the level alignment is rather independent of the experimental details, such as the electronic structure of the oxide, defects in the oxide, and the thickness of oxide and overlayer. The model can also be extended to organic molecules or polymers on metals without any intermediate oxide as long as certain conditions are met. It also sheds new light on the large polaronic binding energy required to interpret the electronic level alignment of metal-polymer interfaces.

1. Introduction

Electronic and optoelectronic devices based on organic semiconductors consist of a number of different chemical components arranged either in layers or intermixed as in heterojunction solar cells.[1–9] The layers provide different functionalities such as light emission or absorption, electron and hole transport, and blocking and contact for electrons and holes, respectively.[7] Contact layers are introduced to facilitate the emission of electrons and holes from the cathode or anode, respectively, into the organic stack. The characteristic quantities for these contacts are the emission barriers for electrons (Φ_{Bn}) and holes (Φ_{Bp}), which the carriers have to overcome when entering the transport levels of the adjacent organic molecule. Hence, these barriers are the energy difference between the Fermi level E_F of the contact material and the transport orbital which usually is the lowest unoccupied molecular orbital (LUMO) for electrons ($\Phi_{Bn} = E_{LUMO} - E_F$) and the highest occupied molecular orbital (HOMO) for holes ($\Phi_{Bp} = E_F - E_{HOMO}$). For a direct contact, (i.e., one without intermediate dielectric between the metal and the organic layer), the barriers are overcome by thermionic emission and therefore even differences of the order of $3kT \approx 75$ meV (at room temperature) make a difference in the contact resistance of more than one order of magnitude. Consequently, the design and characterization of suitable metal/organic molecule combinations in terms of energy level line-up have been and continue to be an area of intense research and development.[10–25] The most-direct information about the energetic positions of the HOMO and LUMO relative to the Fermi level of the contact material comes from photoemission and inverse photoemission work on the metal/organic interfaces. The status of this topic after about twenty years of research has recently been summarized comprehensively by two of the protagonists of this kind of work and their collaborators. They have developed concepts, which not only systematize the large body of experimental work on metal/organic interfaces, but are also meant to have a certain predictive value for the tailoring of these interfaces.[26,27] The concepts owe much to the older concepts developed in conjunction with corresponding contact problems in the area of Schottky and ohmic contacts to inorganic semiconductors.[28]

The starting point is in both cases the Schottky–Mott rule, whereby the vacuum level E_{vac} is the common energy level for the line-up of those of a metal (for simplicity we will refer to all kinds of contact material as metal even though in organic electronics highly conducting and transparent materials such as indium tin oxide (ITO) or poly(3,4-ethylenedioxythiophene)-poly(styrenesulfonate) (PEDOT-PSS) are also used) and semiconductor (SC) or organic molecule. If the interaction between the metal substrate and the SC remains weak after deposition, as is the case, for example, for a predominantly Van der Waals interaction, this common reference level determines the barriers according to Equation 1:

$$\Phi_{Bn} = \Phi_{sub} - EA_{org} \text{ and } \Phi_{Bp} = IE_{org} - \Phi_{sub} \quad (1)$$

Here, $\Phi_{sub} = E_{VAC} - E_F$ is the work function of the metal substrate and $EA_{org} = E_{VAC} - E_{LUMO}$ and $IE_{org} = E_{VAC} - E_{HOMO}$ are

Prof. L. Ley, Prof. J. Ristein
Institut für Technische Physik
Universität Erlangen
D-91058 Erlangen, Germany
E-mail: lothar.ley@physik.uni-erlangen.de
juergen.ristein@physik.uni-erlangen.de
Prof. L. Ley, Y. Smets, Dr. C. I. Pakes
Department of Physics
La Trobe University
Bundoora, Victoria 3086, Australia

DOI: 10.1002/adfm.201201412

the electron affinity and ionization energy of the organic semiconductor, respectively, as they are measured for the isolated constituents of the interface. This, of course, presupposes that the LUMO and HOMO are the transport levels for electrons and holes, respectively. An obvious consequence of the Schottky–Mott rule is that the work function remains unchanged after deposition of the organic semiconductor onto the substrate, that is to say:

$$\Phi_{sub,org} = \Phi_{sub} \quad (2)$$

Consequently, varying the substrate work function for a common organic overlayer will change the barrier height and the work function by the same amount:

$$\frac{d\Phi_{sub,org}}{d\Phi_{sub}} = \frac{d\Phi_B}{d\Phi_{sub}} = S = 1 \quad (3)$$

Thus, the slope parameter, S, equals unity.

For stronger interacting systems the slope parameter is smaller than 1 and might even approach 0. This is the situation referred to as "pinning of E_F" and the consequence for the work function of the combined system of the substrate and an organic overlayer is that it deviates from the substrate work function by an energy $\Delta\Phi$:

$$\Phi_{sub,org} = \Phi_{sub} + \Delta\Phi \quad (4)$$

"Ideal" interfaces (i.e., one that follows the Schottky–Mott rule ($S = 1$)) have regularly been observed by Salaneck and co-workers for polymers deposited by spin-coating onto metal surfaces,[26] whereas a pinning situation with $S < 1$ has more often been observed for small organic molecules evaporated under ultra high vacuum (UHV) conditions onto metals by the groups of Kahn, Ueno, and Koch.[10,12,15–24,27]

However, even for polymers on metals there occurs a transition from $S = 1$ to $S = 0$ when the frontier orbitals approach the Fermi level to, within an energy γ, the HOMO from below and the LUMO from above, or in other words, if $IE_{org} - \Phi_{sub} < \gamma$ or $\Phi_{sub} - EA_{org} < \gamma$. In the work of Salaneck and co workers,[26] this results in what they refer to as the "Zorro" curve of **Figure 1**. For an explanation they invoke a transfer of integer charges between the substrate and the polymer. The level into which electrons or holes are transferred are called integer charge transfer states ($ICT^{+,-}$), where the superscript indicates the sign of the charge transferred. The transferred charge sets up an electric field between the substrate and the overlayer and a corresponding potential step $\Delta\Phi$. $\Delta\Phi$ varies by the same amount as Φ_{sub} such that E_F remains pinned at the corresponding ICT and no variation in the combined work function of the polymer on the substrate is observed for different metals. Experimentally in the work of Salaneck and co-workers, the energies of the ICTs relative to the vacuum level equal the work function of the substrate at the intersection of the $S = 1$ and $S = 0$ branches of the Zorro curve as indicated in Figure 1. However, a difference γ of about 0.4 to 0.6 eV is regularly measured between the energies of the ICTs so determined and E_{HOMO} and E_{LUMO}, respectively. In other words, the Fermi level is not pinned directly at the HOMO or LUMO but remains separated by an energy γ. This difference is ascribed by the authors to polaronic effects, which

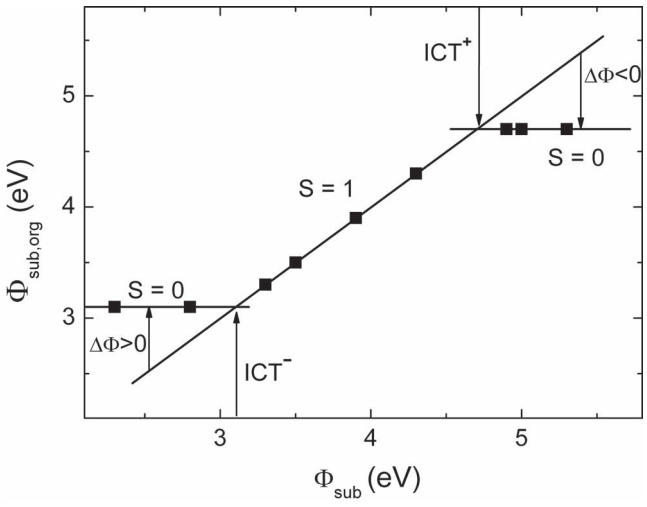

Figure 1. So-called "Zorro" diagram according to Salaneck and co-workers.[26] Fictitious data points of the combined work function $\Phi_{sub,org}$ of an organic layer on top of different substrates are plotted vs. the substrate work function Φ_{sub}. The intersections of the $S = 1$ branch with the two $S = 0$ branches mark the energies of the integer charge transfer states $ICT^{+,-}$. The energy differences $\Delta\Phi$ are marked by arrows.

are not included in the spectroscopically determined HOMO and LUMO energies as expressed through IE_{org} and EA_{org}, respectively. The unusually large polaronic binding energy is, according to the authors, due to the fact that one is dealing here with interface polarons. We shall return to this question later.

Recently, Greiner et al.[29] expanded the results of Salaneck and co-workers[26] to encompass small molecules as well. They too observed the upper part of the Zorro curve for a great number of organic/metal oxide molecule interfaces, albeit measured slightly differently. Instead of the work function, they measured the energy of the HOMO orbital relative to E_F, (i.e., the hole-emission barrier Φ_{Bp}), and plotted $\Delta E_H = \Phi_{Bp} = E_F - E_{HOMO}$ vs. $\Phi_{sub} - IE_{org}$. This plot is redrawn here as **Figure 2**. Substrates and interfaces were prepared in UHV and the substrate work function, the ionization energy of the organic molecules, and ΔE_H were measured in situ by photoemission spectroscopy. In this sense, Greiner et al.'s[29] procedure follows more closely that of Kahn and co-workers,[27] except for using metal substrates with a well-defined oxide layer on top. Nevertheless, the experimental results comply perfectly with those of Salaneck and co-workers and the interpretation is based on the same concept, namely the transition from the Schottky–Mott regime to pinning when the substrate work function equals the ionization energy:

$$\begin{aligned} S &= 1 \quad \text{for} \quad \Phi_{sub} - IE_{org} \leq 0 \\ S &= 0 \quad \text{for} \quad \Phi_{sub} - IE_{org} \geq 0 \end{aligned} \quad (5)$$

The transition at $\Phi_{sub} - IE_{org} = 0$, as suggested by the dashed line, indicates that the relevant ICT^+ is indeed the HOMO. However, spectroscopically the HOMO is measured about 0.3 eV below E_F. Greiner et al.[29] were able to describe their considerable body of data with an expression that contains four adjustable parameters. In what follows, we present a

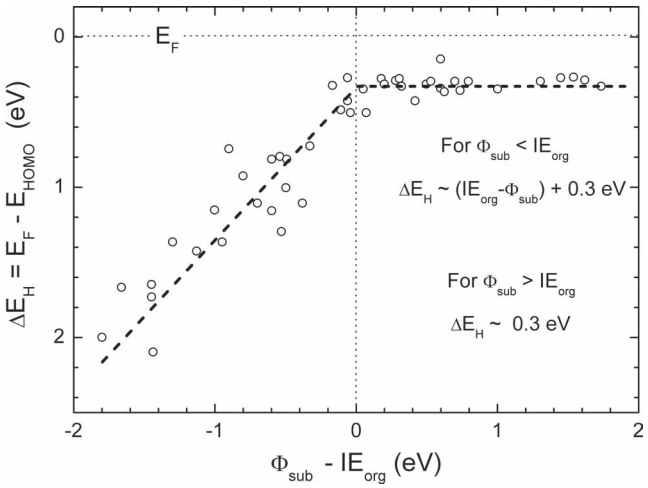

Figure 2. Level alignment of about 40 organic/metal oxide interfaces as measured by Greiner et al.[29] The dashed lines are best fits with slope 1 and slope 0, respectively, as indicated by Greiner et al.[29] Adapted with permission.[29] Copyright 2011, Macmillan Publishers Ltd: Nature Materials.

simple, physically reasonable model that allows for the description of Greiner et al.'s results without any adjustable parameters. It furthermore sheds some new light on the polaronic energy difference, γ, in the work of Salaneck, Fahlmann, and others.[13,14,25,26]

2. Results and Discussion

2.1. Greiner et al.'s Formula

Greiner et al.'s[29] formula describing the connection between $E_F - E_{HOMO}$ on one side and the difference between the substrate work function Φ_{sub} and the ionization energy IE_{org} of the molecule on the other, reads

$$\Delta E_H = E_F - E_{HOMO} = IE_{org} + \delta - \alpha\Phi_{sub} + \frac{e^2\rho d}{2\varepsilon_0}\sum_{i=0}^{\infty}\left(1 + g\exp\left[\frac{IE_{org} - (\Phi_{sub} - i\beta)}{kT}\right]\right)^{-1} \quad (6)$$

The parameters that enter into Equation 6 and their meaning according to ref.[29] are the following: "…δ is the interfacial dipole from the "push-back" effect, α is a proportionality constant based on the molecular layer's ability to screen the potential of the substrate surface, Φ_{sub} is the substrate's work function, e is the elementary charge, ρ is the planar number density of molecules and d is the distance between the molecular plane and the substrate. The summation is taken over i molecular layers." The parameter g is the degeneracy factor of the HOMO level, and all of the other symbols have their usual meaning, apart from β, whose meaning is described below. The gist of the underlying physical model is given as: "the above model implies that pinning occurs because, when a molecule is adsorbed to a surface and coupled with the solid's Fermi energy, the ionized form of the molecule becomes thermodynamically stable when the Fermi energy [or better, the work function] is greater than the ionization energy."

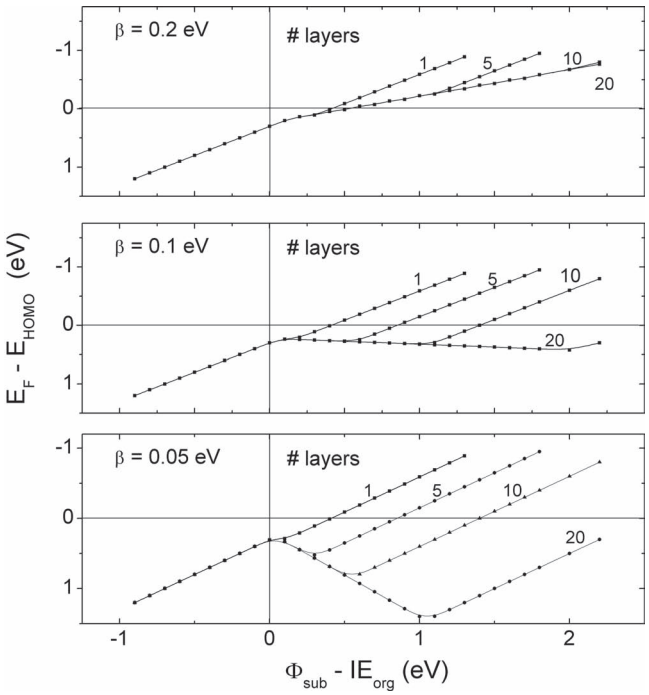

Figure 3. Evaluation of Equation 6 for 1, 5, 10, and 20 layers of organic molecules and three values of β.

The authors were so generous to provide us with the values of the parameters they used to generate the dashed line in Figure 2 from Equation 6. They are 0.22 eV for δ, 0.11 eV for the prefactor to the sum and 0.1 eV for β. The slope parameter γ equals 1, as estimated from the slope of the dashed line in Figure 2. With these parameters we have evaluated Equation 6 for different numbers of layers of organic molecules. We have also varied the crucial parameter β between 0.05 eV and 0.2 eV. The result is shown in **Figure 3**.

Referring firstly to the curves for $\beta = 0.1$ eV, it is apparent that with increasing difference in $\Phi_{sub} - IE_{org}$ an increasing number of organic layers is required to yield the pinning of E_{HOMO} to a level about 0.3 eV below E_F. For a difference of 1.9 eV, which corresponds, for example, to 4,4′,4″-tris(*N*-2-naphthyl-*N*-phenyl-amino)triphenylamine (2T-NATA) (IE_{org} = 4.98 eV) on V_2O_5 (Φ_{sub} = 6.9 eV) a thickness of at least 20 layers would be required before a pinning of E_{HOMO} should be observed. That corresponds to an overlayer thickness of approximately 160 Å, while the data points in Figure 2 were obtained for about a monolayer of organic molecules.[29] Hence, a summation over an infinite number of layers as implied by Equation 6 in the form given by Greiner et al.[29] does indeed reproduce the pinning position but is physically unreasonable. The difference of 0.3 eV in $E_F - E_{HOMO}$ is furthermore determined solely by the "push-back" parameter δ according to Equation 6. What appears to be missing in the diagram of Greiner et al. (Figure 2) is the slight but systematic increase in $E_F - E_{HOMO}$ in the region $\Phi_{sub} - IE_{org} > 0$ that is undoubtedly present in the evaluation of Equation 6 with the parameters provided by Greiner. The result is, furthermore, very sensitive to the parameter β. For $\beta > 0.1$ eV there is no pinning at all and for $\beta = 0.05$ eV there

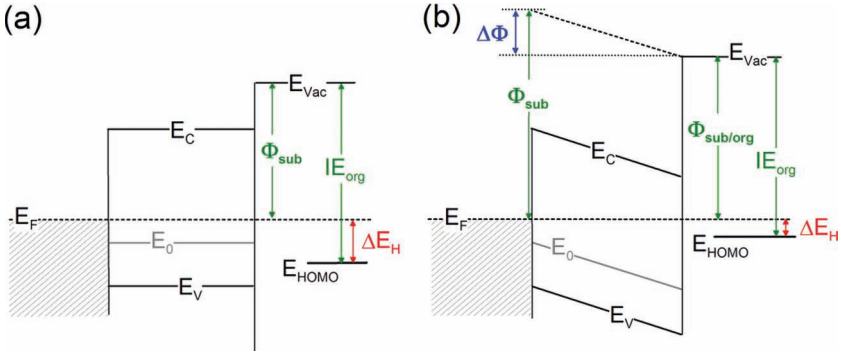

Figure 4. Schematic band diagrams illustrating for the Schottky–Mott rule the Schottky–Mott regime (a) and the pinning case (b) for the HOMO position in a metal/oxide/organic interface. All of the energy differences that are marked by the arrows are positive throughout the paper. We have sketched the two cases for the same organic molecule (i.e., identical IE_{org}, but different substrate work functions Φ_{sub}). Note that in each case only the difference between these two quantities is physically relevant. The charge neutrality level E_0 of the oxide should be used when defects within the oxide are taken into account.

is an overcompensation of the screening and an entirely unrealistic dependence of E_{HOMO} on the difference $\Phi_{sub} - IE_{org}$. It is thus hard to imagine a reasonable physical origin of the parameter β that would explain the extreme sensitivity of the HOMO position on the exact value of this parameter, and that would have to be exactly the same for all organic/metal oxide heterojunctions. We have therefore analyzed the problem ex ovo and our approach will be described next. We will restrict the discussion to the case of p-type organic overlayers, as it is also exclusively discussed in the work by Greiner et al. Conceptually however, electron injection into the LUMO of organics with sufficiently high electron affinity can be dealt with in strict analogy.

2.2. Charge Transfer and Level Alignment

2.2.1. The Oxide as an Ideal Dielectric

We start by assuming that the interaction between substrate and organic layer is so weak that there are no changes in level alignment due to short-range interface dipoles upon contact between the molecule and the substrate. We shall refer to this situation as governed by the Schottky–Mott rule as opposed to the situation where intimate contact between the molecule and the substrate sets up dipoles on an atomic scale, which modify the line-up of the substrate work function, Φ_{sub}, and molecule ionization energy, IE_{org}, as they are measured separately. This is a more-stringent assumption than that of Greiner et al.[29] because their parameter δ allows just that, namely a change of Φ_{sub} brought about by the contact between molecule and oxide. To be distinguished from the Schottky–Mott rule is the Schottky–Mott regime, which corresponds to the situation where the HOMO position is well below E_F, and hence no net charge exchange occurs between substrate and molecules. In this regime (see **Figure 4**a), the energy difference between E_F and E_{HOMO} scales linearly with $\Phi_{sub} - IE_{org}$, as observed experimentally for $\Phi_{sub} - IE_{org} < 0$ by Greiner et al. We agree with Greiner et al. that a charge transfer from the HOMO level to E_F occurs once the former approaches or exceeds the latter. Whereas Greiner et al. make no statement as to where the electrons from the organic HOMO are transferred, we postulate that they are transferred to the metal because there are, in most cases, no accessible empty states in the oxide. This is assuming that the oxide layer behaves as a perfect dielectric with no defect states in the band gap and with valence and conduction band edges far from the Fermi level, so that the density of free charge carriers is negligible. The positive charge, Q, (per unit area) in the organic adlayer must then be compensated by an equal but opposite negative charge in the metal. The oxide in between acts purely as a dielectric and hence a potential difference

$$\Delta\Phi = e\frac{Q}{C_{ox}} \tag{7}$$

develops across the oxide, where $C_{ox} = \frac{\varepsilon\varepsilon_0}{d_{ox}}$ is the capacitance per unit area of the metal/organic layer slab with the oxide (relative permittivity ε) of thickness d_{ox} as a dielectric in between (cf. Figure 4b).

In a first step we will assume that the organic layer deposited onto the substrate is so thin that any potential drop across it can be neglected. We will discuss the error caused by this approximation further below. Q, the positive areal charge in the HOMOs of the organic adlayer is determined by the product of the areal molecular density n and the probability of the HOMO to accommodate a hole, (i.e., by. $[1 - FD(E_{HOMO} - E_F)]$ where FD is the Fermi–Dirac function augmented by the degeneracy factor g of the HOMO). With $E_{HOMO} - E_F = (\Phi_{sub} - \Delta\Phi) - IE_{org}$ (see Figure 4), the following expression holds for the total positive areal charge density Q residing in the HOMO levels of the adsorbed molecules:

$$\begin{aligned} Q &= en\left(1 - \left[1 + g^{-1}\exp\left(\frac{\Phi_{sub} - \Delta\Phi - IE_{org}}{kT}\right)\right]^{-1}\right) \\ &= en\left[1 + g\exp\left(\frac{IE_{org} - \Phi_{sub} + \Delta\Phi}{kT}\right)\right]^{-1} \\ &= en\left[1 + \exp\left(\frac{(IE_{org} - \Phi_{sub} + kT\ln g) + \Delta\Phi}{kT}\right)\right]^{-1} \end{aligned} \tag{8}$$

Here, g is the degeneracy factor of the HOMO. The FD function in Equation 8 applies to the ensemble of molecules such that each molecule has either one or no positive charge in order to yield, on average, the fractional occupancy as required by the FD statistics. Note that the degeneracy factor g of the HOMO causes a weak logarithmic temperature-dependent shift of the energy difference $IE - \Phi_{sub}$. By inverting Equation 7 and combining with Equation 8 the charge-neutrality condition yields an implicit equation for the potential drop, $\Delta\Phi$, across the oxide:

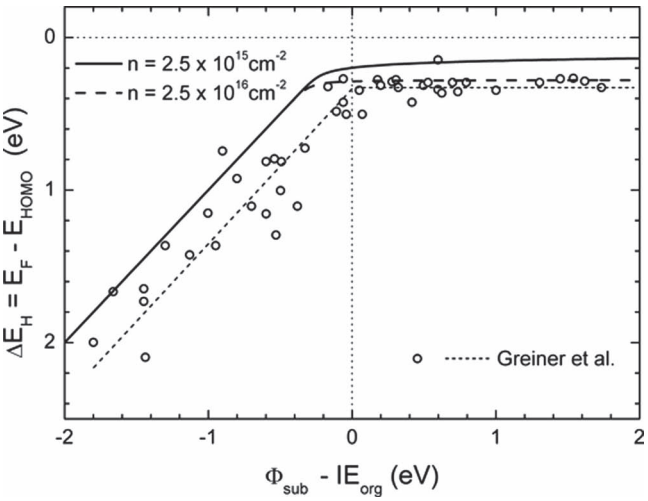

Figure 5. $E_F - E_{HOMO}$ vs. $\Phi_{sub} - IE_{org}$ as calculated in the framework of the charge-transfer model for one (solid line) and 10 (dashed line) monolayers of organic molecules on top of an oxide, according to Equation 9a. The data and fits of Figure 2 are also plotted in grey.

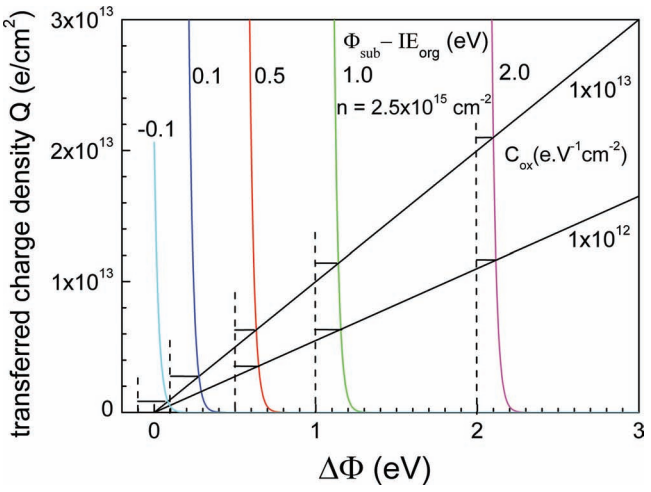

Figure 6. Graphical solution of Equation 7 and 8. The straight lines are the transferred charge Q vs. $\Delta\Phi$ from the capacitor Equation 7, calculated for two capacitances C_{ox} that differ by an order of magnitude. They cross the tails of the *FD* function ($g = 1$), Equation 8, also plotted as a function of $\Delta\Phi$ with different values for $\Phi_{sub} - IE_{org}$ as a parameter. The dashed lines mark the Fermi level positions and the distance from there to the corresponding crossing point (short horizontal lines) give the distance between E_F and E_{HOMO}.

$$\Delta\Phi = e^2 \frac{n}{C_{ox}} \left[1 + g \exp\left(\frac{IE_{org} - \Phi_{sub} + \Delta\Phi}{kT}\right)\right]^{-1} = \Phi_0 \left[1 + g \exp\left(\frac{IE_{org} - \Phi_{sub} + \Delta\Phi}{kT}\right)\right]^{-1} \quad (9a)$$

Aside from the weak influence of the HOMO degeneracy, the solution of Equation 9 for a specific energy difference $IE_{org} - \Phi_{sub}$ depends only on one system parameter, Φ_0, which is, up to e^2, the ratio of the organic surface coverage n and the oxide capacitance C_{ox}.

In **Figure 5** we have plotted ΔE_H vs. $\Phi_{sub} - IE_{org}$ by solving Equation 9a for $g = 1$ and typical system parameters as used by Greiner et al.:[29] an oxide thickness of 6 nm and 6 for the permittivity of the oxide layer, giving $C_{ox} = 8.85 \times 10^{-3}$ F cm^{-2} = 5.5×10^{12} e cm^{-2} V^{-1}. The coverage of organic molecules was set to one monolayer or 2.5×10^{15} cm^{-2}, corresponding to the experimental situation. Comparison with Figure 2 shows that our model reproduces the trend in the data just as well as Greiner et al.'s formula for an infinite number of layers albeit without any adjustable parameters: the Schottky–Mott regime with slope parameter $|\gamma| = S = 1$ for $IE_{org} > \Phi_{sub}$ and a HOMO level that is pinned between 0.14 and 0.2 eV below E_F for $\Phi_{sub} > IE_{org}$.

A pinning position of E_F more than $10kT$ above E_{HOMO} was one of the surprising results in the work of Greiner et al.[29] because, for situations where the Schottky–Mott rule holds, the pinning position was assumed to coincide with the ICT$^+$, which, in the present case, coincides with the HOMO experimentally, as well as in our model calculation. The experimental evidence is the fact that the $S = 1$ and $S = 0$ branches cross at $\Phi_{sub} = IE_{org}$ in Figure 2 as mentioned earlier.

In order to gain some insight into the origin of this offset in the pinning regime, we have plotted in **Figure 6** the two charge densities separately: the positive charge density Q^+ in the molecules, which is governed by the *FD* function, and the negative charge density Q^- in the metal, which is related to the potential drop $\Delta\Phi$ via Equation 7 by a linear relationship with C_{ox} as the slope.

Equation 7 and 8 have to be fulfilled simultaneously for a common Q. The ensuing condition in terms of Q and $\Delta\Phi$ corresponds to the crossing points shown in Figure 6 for a range of $\Phi_{sub} - IE_{org}$ values. In Figure 6, we have bracketed the nominal C_{ox} value of 5.5×10^{12} e cm^{-2} V^{-1} by $C_{ox} = 1 \times 10^{12}$ and $C_{ox} = 1 \times 10^{13}$ e cm^{-2} V^{-1} to account for uncertainties in d_{ox} and ε. From Figure 6 it is apparent that the crossing points between the two functions for Q occur in the tail of the *FD* distribution rather than at E_F, the point where the average occupation of the HOMO levels is 0.5. This is due to the fact that, even for large differences $\Phi_{sub} - IE_{org}$ on average, a hole concentration per molecule well below 0.5 is sufficient to fulfill the charge equilibrium between the metal and the molecular layer (see also **Figure 7**). As a consequence, the crossing points do not coincide with $\Phi_{sub} = IE_{org}$, but occur rather at a value that is about 0.2 eV above.

Rather than exploring a large parameter space to see how the ΔE_H offset varies with system properties, we turn to a closer inspection of Equation 9a. Using the parameters quoted above, the prefactor $\Phi_0 = e^2 n / C_{ox} = 1100$ eV. The pinning value can be estimated when we read Equation 9a as a self-consistent equation for $\Delta E_H = IE_{org} - \Phi_{sub} + \Delta\Phi$ (cf. Figure 4b):

$$\Delta E_H + \Phi_{sub} - IE_{org} = \Phi_0 \left[1 + g \exp\left(\frac{IE_{org} - \Phi_{sub} + \Delta\Phi}{kT}\right)\right]^{-1} \quad (9b)$$

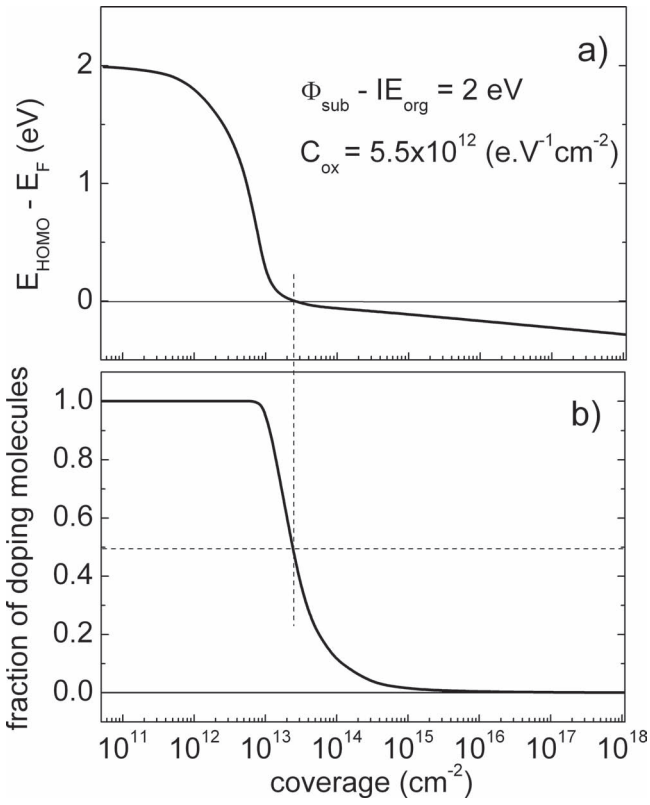

Figure 7. a) $E_{HOMO} - E_F$ as a function of coverage. b) The fraction of molecules that is simply positively charged as a function of coverage.

$$\Delta E_H = kT \ln\left[g^{-1}\left(\frac{\Phi_0}{\Phi_{sub} - IE_{org} + \Delta E_H} - 1\right)\right]$$
$$\approx kT \ln\left(\frac{\Phi_0/g}{\Phi_{sub} - IE_{org}}\right) \quad (10)$$

In the last step we have used $\Phi_0 \gg \Phi_{sub} - IE_{org} \gg \Delta E_H$. For $\Phi_{sub} - IE_{org} = 2.0$ eV and $g = 1$ we obtain $\Delta E_H = 0.158$ eV as an approximate solution for the pinning position. This is small compared with $\Phi_{sub} - IE_{org}$ justifying the approximation, and indistinguishable from the value read from Figure 5. From Equation 10 it is obvious that ΔE_H shows only a weak logarithmic dependence on $\Phi_{sub} - IE_{org}$ and on all other system parameters gathered in Φ_0 except for the temperature. Even for a close contact of an organic layer with a metal surface which is equivalent to setting the oxide thickness to a molecular scale of say 0.3 nm, Φ_0 is reduced only to 55 eV, still larger than any reasonable difference $\Phi_{sub} - IE_{org}$. Equation 10 thus holds for the pinning position also in the absence of an oxide. However, even in this situation the Schottky–Mott rule is supposed to prevail and pinning is solely brought about by integer charge transfer between the substrate and the molecule and the ensuing potential difference $\Delta\Phi$ across a space of molecular dimensions. Reducing the thickness of the dielectric layer by a factor of 20 goes along with a reduction of ΔE_H by $kT\ln(20) = 75$ meV, illustrating once more the weak logarithmic dependence of the pinning position on the system parameters.

2.2.2. The Charge Distribution in the Molecular Layer

It is furthermore instructive to follow the evolution in charge transfer and $E_F - E_{HOMO}$ as a function of coverage in the pinning regime. This is done in Figure 7a for $\Phi_{sub} - IE_{org} = 2$ eV and the experimental value of C_{ox}. Also shown, in Figure 7b, is the fraction of molecules that are positively charged on account of the charge transfer. The initial difference between E_{HOMO} and E_F is 2 eV and all molecules deposited are positively charged on account of the large difference between E_{HOMO} and E_F, which is only gradually reduced by the potential drop $\Delta\Phi$ across the oxide capacitor. However, for $C_{ox} = 5.5 \times 10^{12}$ eV^{-1} cm^{-2}, a coverage of only 2.2×10^{13} cm^{-2} suffices to donate the amount of charge needed to lower E_{HOMO} to the position of E_F, and the average number of charged molecules has dropped to 0.5. This coverage corresponds approximately to 1/100th of a monolayer (ML). For a coverage of 2.5×10^{15} cm^{-2} (1 ML), which is the thickness typically used in the data of Figure 2, the average occupation of the HOMO levels with positive charge has dropped to 4×10^{-3}. This means that about one out of 250 organic molecules is actually charged in order to maintain the amount of transferred charge that is necessary to yield a $\Delta\Phi$ that is large enough to keep E_{HOMO} close to but somewhat below E_F. It is this fact that allows a position of E_{HOMO} in the tail of the *FD* distribution and that is responsible for the 0.14 eV difference between E_F and E_{HOMO}, which is consistently observed in the work of Greiner et al.[29]

The analysis considered here for the pinning of E_F at the HOMO in cases where $\Phi_{sub} > IE_{org}$, holds also for the pinning of E_F at the LUMO for substrates with very low work functions ($\Phi_{sub} < EA_{org}$). For example, the gradual transition from fully ionized organic molecules to mainly neutral molecules has recently been observed for $C_{60}F_{48}$ on diamond, where a charge transfer from the diamond to the LUMO of the $C_{60}F_{48}$ takes place and leads to the well-known surface conductivity of hydrogen-terminated diamond that is carried by a hole accumulation layer below the diamond surface. In this case, the different charge states of $C_{60}F_{48}$ have been identified and quantified through a marked chemical shift in the C1s core level spectrum of charged and neutral $C_{60}F_{48}$ species.[30] An indication of differently charged overlayer molecules has also been seen in the valence-band spectra of C_{60} on poly(3-hexylthiophene) (PH3T).[14]

2.2.3. The Effect of a Finite Thickness of the Organic Layer on the Pinning Position

With the parameters of Greiner et al.'s[29] experiment, specifically by setting the organic layer thickness to 0.40 nm corresponding to 1 ML (2.5×10^{15} cm^{-2}), as specified by the authors, we obtain a pinning position of $\Delta E_H = 0.14$ eV compared with the experimental value of 0.33 ± 0.05 eV in ref.[29] In this and the following we shall refer to ΔE_H at $\Phi_{sub} - IE_{org} = 2$ eV as the "pinning position". One possible origin for this systematic deviation could be due to the polaronic effect suggested by Salaneck and co-workers[26] to explain a similar offset in their ICT$^+$ compared with E_{HOMO} in polymer/metal interfaces.[29] It is an open question if such an explanation can hold also for the smaller molecules used in the study of Greiner et al. An

alternative possibility is that the real thickness of the organic layer was underestimated in the experiment and hence in our simulation. In the Supporting Information to ref.[29], Greiner et al. in fact show spectra for organic layer thicknesses up to 12 nm, and their model reproduced here as Equation 6 explicitly takes an infinite number of organic layers into account. We will therefore extend our model in the same sense; that is to say, by evaluating the electric-field profile in the organic layer. In order to do so, we once more consider Equation 8 for the total areal charge density in the organic layer. It is up to a factor e/C_{ox}, identical to the right hand side of Equation 9, which determines the potential drop between the metal surface and the surface of the oxide layer. So far, we have assumed that the organic layer has zero thickness and $IE_{org} - \Phi_{sub} + \Delta\Phi$ in Equations 8 and 9 is the Fermi level position relative to the HOMO, valid for all organic molecules. When the organic sheet is built up from more than one (say M) molecular layers, each with a molecule density ν and separated by a distance d from each other; this energy, and thus the potential difference Φ_M vs. the metal substrate have to be calculated separately to obtain the correct areal charge density δQ_M in each layer. According to Gauss' law of electrostatics, the areal charge density in a specific layer, m, in turn reduces the electric field in the space between this and the next layer of the stack by $\Delta F_{m+1,m} = \delta Q_m/(\varepsilon_0\varepsilon_{org})$ where ε_{org} is the permittivity of the molecular solid. The potential difference between the m^{th} and the $m + 1^{th}$ layer is $-F_m d$ and that gives the following recursion scheme by which the fields F_m and potentials, Φ_m, of the M layers must be evaluated:

$$\Phi_{m+1} = \Phi_m + eF_m d \quad \text{and}$$
$$F_{m+1} = F_m - \frac{e\nu}{\varepsilon_0\varepsilon_{org}}\left[1 + g\exp\left(\frac{IE_{org} - \Phi_{sub} + \Phi_m}{kT}\right)\right]^{-1} \tag{11a}$$

with the initial values:

$$\Phi_0 = \Delta\Phi = \frac{eQ}{C_{ox}} \quad \text{and} \quad F_0 = \frac{\Delta\Phi}{ed_{ox}}\cdot\frac{\varepsilon_{ox}}{\varepsilon_{org}} \tag{11b}$$

When the top molecular layer is not complete, the areal molecular density ν has to be reduced for this layer accordingly. The condition of charge neutrality in this recursion scheme is equivalent to $F_{M+1} = 0$ (i.e., a vanishing field at the surface of the organic layer), and $\Delta\Phi$ has to be determined to match this condition.

In **Figure 8** we have evaluated the pinning position ΔE_H (full curve) as a function of the organic layer thickness for d = 0.40 nm and $\varepsilon_{org} = 2.5$.

The dashed line in Figure 8 reproduces the result of Figure 7 when we follow the simple model of Equation 9, ignoring the potential drop in the organic layer. This can easily be achieved also in the recursion formula (Equation 12) by formally setting $d = 0$. We start by considering the full calculation for the case of an oxide thickness of 6 nm (full line in Figure 8). For coverages up to a monolayer (ML), both models, that with and that without consideration of the potential drop within the molecular layer, give identical results, as would be expected. However, beyond a ML, the increase in ΔE_H with number of layers is clearly more pronounced when the potential drop in the organic layer is taken properly into account. For 4 nm, we

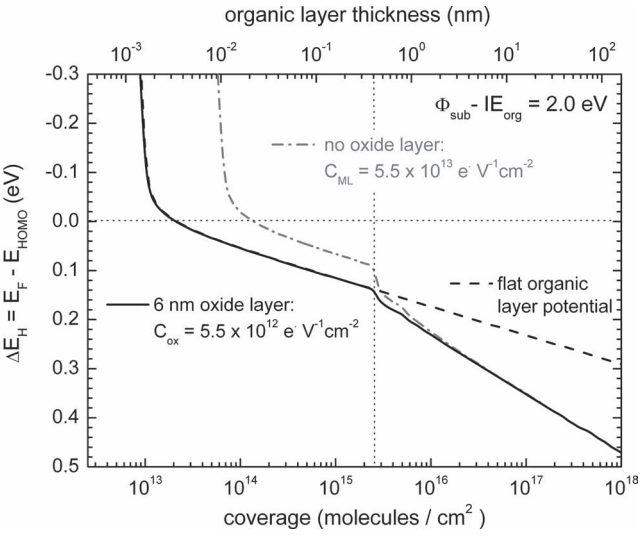

Figure 8. $E_F - E_{HOMO}$ as a function of coverage in the pinning regime $\Phi_{sub} - IE_{org} = 2.0$ eV. The full and dash-dotted lines represent the full model including the potential profile in the molecular layer stack: solid line for a 6 nm oxide and dash-dotted line for no intermediate oxide. C_{ML} in the latter case denotes the interface capacitance between the metal surface and a molecular monolayer. The dashed line reproduces the oxide case of Figure 7, which ignores the potential profile in the organic layer. The dotted vertical line marks the monolayer coverage.

calculate $\Delta E_H = 0.28$ eV and, for $d = 11$ nm, corresponding to the maximum thickness investigated by Greiner et al. (see supporting information to ref.[29]), we find $\Delta E_H = 0.33$ eV (instead of the 0.14 eV for a single layer), which is identical to the experimental value of 0.33 ± 0.05 eV. The 4 nm case is also plotted in Figure 5 as the dashed line.

We proceed by discussing the "non-oxide" case, where we assume a distance of closest approach between the organic layer and metal of 0.25 nm and a permittivity of 2.5, resulting in a capacitance $C_{ML} = 10C_{ox}$. Here, the larger capacitance of the interface requires more charge transfer to pull the surface HOMO close to the Fermi level. Consequently, about 3% of an organic monolayer is now needed to pin E_F at E_{HOMO}, and, for 1 ML coverage, $\Delta E_H = 0.08$ eV is noticeably smaller than in the oxide case ($\Delta E_H = 0.14$ eV). With an increasing number of organic layers, however, the pinning value, ΔE_H, increases and is practically identical to the oxide case for three layers of organic molecules. Hence, for organic layers beyond a few MLs the thickness of the oxide has no influence on the pinning position.

We should make a comment on the electric fields that go along with the pinning mechanism in the case of the "no oxide" metal/organic interfaces: without a separating dielectric, the potential difference between the metal and the organic layer is set up across a molecular distance, say typically 0.25 nm, as we have assumed in our simulation. Pinning from an original level separation of $\Phi_{sub} - IE_{org} = 2.0$ eV leads to an electric field of 80 MV cm^{-1} between the metal and the organic layer. This value is about four times the break-down field in diamond (≈ 20 MV cm^{-1}) known as the strongest dielectric so far.[31] This is an interesting aspect with respect to the limits of the model

presented here. We do not want to discuss this further, but mention only that electric break-down fields in matter conceptually do not limit electric fields on a molecular scale.

2.2.4. The Effect of a Finite Density of Defects in the Oxide Layer

The final question to be answered is how the electrons get from the HOMO of the adlayer to the metal. From an operational point of view, it is clear that the oxides provide the necessary conductance to enable the electron transfer in a fraction of a second. This is so because in the photoemission spectra of Greiner et al.[29] there is no measurable charging shift. Whenever electrons are emitted from the surface of a sample, they have to be replenished from the back contact, which is in electrical contact with the spectrometer. This current causes a potential drop between surface and the back contact, which is a product of the electron current and the sample resistance. Such a potential drop, if measurable, is referred to as a "charging shift". The photoelectron current in the kind of experiments performed by Greiner et al.[29] is of the order of 10^{-9} A from an illuminated spot of about 1 mm diameter, or about 10^{-7} A cm^{-2}. The smallest measurable shift is estimated to be about 50 meV. This implies that the oxide resistance over an area of 1 cm^2 is of the order of 5×10^5 Ω or smaller. This maximum sample resistance compatible with the experimental observations corresponds to a lower limit of 1.2×10^{-12} Ω^{-1} cm^{-1} for the conductivity of the oxide layer. Hence, in the worst case, it takes about 1 s to transfer the 10^{13} e cm^{-2} that are necessary to pin E_{HOMO} across the oxide for an initial potential difference of 1 V (cf. Figure 6).

The obvious mechanism for a current across a wide-bandgap dielectric is quantum-mechanical tunnelling through the oxide. In lieu of data for the oxides used by Greiner et al.,[29] we take models and calculations from metal oxide-semiconductor (MOS) devices as a guide for the tunnelling currents that can be expected in the situation at hand, namely oxides with a thickness of 6 ± 1 nm. The leakage current through a SiO_2 gate oxide of 6 nm thickness at an applied voltage of 1 V is of the order of 10^{-20} A cm^{-2} or about 0.06 e s^{-1} cm^{-2}.[32] This is definitely too small in order to establish the transfer of about 10^{13} e cm^{-2} alluded to above. Hence, there has to be a finite density of deep defect states that carry the transfer current and the photoemission current by hopping conductivity. The most-general expression for hopping conductivity between localized centres that are on average a distance R apart yields a conductivity

$$\sigma = \sigma_0 \exp\left[-\frac{\tau R}{a}\right] \exp\left[-\frac{E_a}{kT}\right] \tag{12}$$

where a is the localization length of the impurity wave function and τ is a numerical factor of order unity. It is generally found that the hopping activation energy E_a lies between 10^{-4} and 10^{-3} eV and the localization length is of the order of 5 nm.[33]

Using these values and $\sigma_0 = 600$ Ω^{-1} cm^{-1} from the work of Fritzsche and Cuevas,[34] we estimate the average distance $R \approx 170$ nm corresponding to an impurity concentration N_i of about 2×10^{14} cm^{-3}, which is required to provide the necessary conductivity. This corresponds to an areal density of 10^8 cm^{-2} for a 10 nm-thick oxide, which has to be compared with an areal density of defects of 10^{10} cm^{-2} for the best SiO_2 gate oxide of comparable thickness in MOS technology. It is more than likely that the oxides in the work of Greiner et al.[29] have considerably higher defect and impurity concentrations, and therefore meet the conductance requirements mentioned above under all circumstances. Naturally, a finite density of defects in the oxide will also contribute to the charge distribution in the molecule-oxide-metal stack, and we shall proceed to calculate the effect of this charge on the level alignment.

The formalism we have developed in the previous sections can, in fact, with a few steps be extended to defective dielectrics as well. To this end, we will assume a constant defect density of states D_0 with a charge neutrality level (CNL) E_0 in the bandgap of the oxide. In most cases, the charge neutrality level in a metal oxide on top of the metal itself is below the metal Fermi level by an energy W_0.[29] Consequently, excess electrons, and thus a negative charge density will reside in the oxide. Following the electron potential, $\Phi(x)$, through the oxide using the CNL (i.e., setting $\Phi(x) = E_0(x) - E_F$ for the potential profile in the oxide), will give a space charge density, ρ, that is linked to the local potential $\Phi(x)$ by $\rho(\Phi) = eD_0\Phi$. In this relation we have employed a step function for the Fermi–Dirac occupation statistics of the defects states (i.e., the low temperature limit). With this space charge function, $\rho(\Phi)$, Poisson's equation for the potential profile in the oxide reads:

$$\frac{\varepsilon_0\varepsilon_{ox}}{e}\frac{d^2\Phi}{dx^2} = e\,D_0\Phi \tag{13}$$

The general solution of this homogeneous differential equation of second order contains two integration constants that need to be fixed by two boundary conditions. The first is given by the potential Φ at the metal surface that is identical to $-W_0$. This leaves only one free constant, λ, for the potential profile inside the dielectric, and it is easily seen that:

$$\Phi(x) = W_0\left[\lambda \exp(\mu x) + (1-\lambda)\exp(-\mu x)\right] \tag{14}$$

where the co-ordinate x extends from the metal/oxide interface in a positive direction towards the surface. The constant μ in the exponential is related to the defect density of states D_0 and the permittivity ε_{ox} of the oxide by $\mu = \sqrt{e^2 D_0/(\varepsilon_{ox}\varepsilon_0)}$. Its inverse is an estimate for the minimum oxide thickness necessary to show the effect of defects on the potential profile across the interface. The total potential drop $\Delta\Phi$ across the oxide, and the total areal charge density Q^- of the metal oxide combination (made up by the sheet charge in the metal on the one hand and the space charge in the oxide defects on the other) and the electric field F_0 at the oxide surface can now be expressed by the parameter λ:

$$\Delta\Phi(\lambda) = -W_0\left[\lambda \exp(\mu d_{ox}) + (1-\lambda)\exp(-\mu d_{ox})\right] \tag{15}$$

and

$$\begin{aligned}\varepsilon_{ox}\varepsilon_0 F_0(\lambda) &= -Q^-(\lambda)\\ &= -\frac{\varepsilon_{ox}\varepsilon_0}{e}\mu W_0\left[\lambda\exp(\mu d_{ox}) - (1-\lambda)\exp(-\mu d_{ox})\right]\end{aligned} \tag{16}$$

$Q^-(\lambda)$ is negative and monotonically decreases with λ and it is readily confirmed that $\lambda_0 = (1 + \exp(2\mu d_{ox}))^{-1}$ yields $Q^- = F_0 = 0$ and describes the case of the bare oxide substrate where the

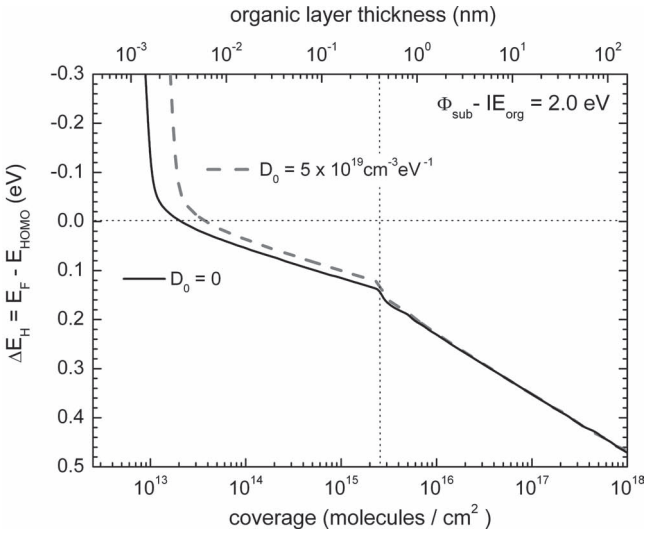

Figure 9. $E_F - E_{HOMO}$ as a function of organic molecule coverage on top of an oxide layer (6 nm) with a high and constant defect density of states D_0 in the band gap (dashed line). For comparison, the surface Fermi level position relative to E_{HOMO} is also shown for the defect-free case (solid line, identical to Figure 8). The dotted vertical line marks the one monolayer coverage.

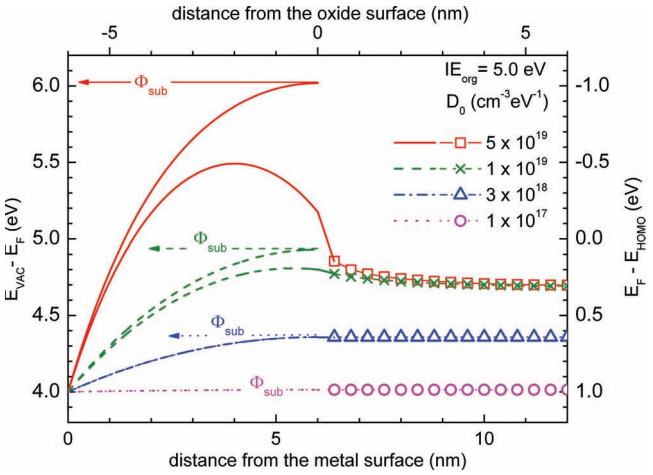

Figure 10. Band profiles for metal/oxide substrates and metal/oxide/organic layer stacks for which the substrate work function is modified by an increase in the density of defect states D_0 in the band gap of the oxide. The arrows labelled Φ_{sub} indicate the varying work functions of the bare substrates. For details see text.

charges in metal and oxide add up to zero. Depositing organic molecules leads to additional negative charge transfer to the substrate and results in potential profiles in the oxide that belong to $\lambda > \lambda_0$. We use λ instead of $\Delta\Phi$ as a variational parameter in the recursion scheme of Equation 9 and replace the starting parameters by:

$$\Phi_0 = \Delta\Phi(\lambda) \text{ and}$$

$$F_0(\lambda) = -\frac{\mu W_0}{e}\frac{\varepsilon_{ox}}{\varepsilon_{org}}\left[\lambda \exp(\mu d_{ox}) - (1-\lambda)\exp(-\mu d_{ox})\right] \quad (17)$$

Again, the variational parameter has to be chosen such that $F_{M+1} = 0$. Φ_M is then the overall potential drop between the metal and the organic layer surface.

We plot in **Figure 9** the surface Fermi level position as a function of the organic layer thickness for this general model that includes defects in the oxide and the full potential profile across the complete interface for an extreme value of the defect density of states in the oxide: $D_0 = 5 \times 10^{19}$ cm^{-3} eV^{-1}. The thickness and permittivity of the oxide, as well as the layer separation and the permittivity of the organic film, are the same as those used in Figure 8 and, for comparison, we have also included the defect-free case from Figure 8 in Figure 9.

The high defect density of states $D_0 = 5 \times 10^{19}$ cm^{-3} eV^{-1} corresponds to $1/\mu = 2.6$ nm, a value comparable with the oxide thickness. For the energy of the oxide CNL relative to E_F, we assume $W_0 = -1.0$ eV with the initial condition $\Phi_{sub} - IE_{org} = 2.0$ eV. As a consequence of the defects in the oxide, the part of the charge in the substrate that is responsible for the pinning is now stored closer to the organic overlayer in the oxide. As a consequence, about twice as many organic molecules are needed to pin E_F at a given level. This is apparent by the horizontal shift in the two curves of Figure 9 for sub-monolayer coverages. However, for coverages beyond 1 ML, the difference is undetectable within the experimental resolution.

While defects in the oxide have no measurable effect on the pinning position, they do alter the potential profile in the oxide significantly as illustrated in **Figure 10**. We simulate a 6 nm oxide, for which we assume densities of defect states that vary between 1×10^{17} cm^{-3} eV^{-1} and 5×10^{19} cm^{-3} eV^{-1}. W_0 is set to –2.5 eV in all cases.

For each D_0 we show two potential profiles. In the ones on the left that end at the oxide surface (6 nm on the lower abscissa), the potential is represented by the vacuum level relative to E_F (left-hand ordinate). The starting point is the work function of the metal, which was set to 4.0 eV. For the lowest D_0, the charge transfer between the metal and the oxide is negligible, resulting in a flat potential across the oxide (dotted line). Consequently, the work function $\Phi_{sub} = (E_{vac} - E_F)_{surf}$ equals that of the metal. Increasing the defect density gradually, however, leads to negative charge transfer from the metal into the oxide and a corresponding upward band bending. This increases the work function of the substrate with increasing D_0 up to 6.0 eV for the highest defect density simulated.

The second set of curves that extend across the whole diagram shows the potential profiles after a 6 nm thick layer of organic molecules with an ionization energy of 5.0 eV was deposited on top of the respective substrates (lines in the oxide, symbols plus lines in the organic layer). The ionization energy was chosen such that $\Phi_{sub} - IE_{org}$ varies between –1.0 eV to and +1.0 eV. This choice was motivated by one of the experiments of Greiner et al.[29] They deposited the same organic molecule (γ-NPD) on top of Ni/NiO substrates, for which they could increase the work function by gradually increasing the density of oxygen interstitial defects by moving to harsher oxidation conditions. As a consequence, they effectively varied $\Phi_{sub} - IE_{org}$ in the range covered by our simulation (–1 eV, +1 eV), and their measured ΔE_H values (their Figure 6) cover the transition from the Schottky–Mott regime to the pinning regime in the

same way as the data of Figure 2. The band profiles in Figure 10 explain this result as well. For low defect densities of states (1×10^{17} cm^{-3} eV^{-1} and 3×10^{18} cm^{-3} eV^{-1}) where the work functions of the substrate remain considerably smaller than IE_{org}, the band profile across the organic layer is flat and the surface Fermi level with respect to the HOMO (ΔE_H, right hand ordinate of Figure 10) simply follows $IE_{org} - \Phi_{sub}$. This is the Schottky–Mott regime, which holds despite substantial band bending in the oxide ($D_0 = 3 \times 10^{18}$ cm^{-3} eV^{-1}). When the defect density becomes so high that the work function approaches or exceeds IE_{org}, the pinning regime is recognized with ΔE_H = 0.33 eV as discussed above. For the extreme case of D_0 = 5×10^{19} cm^{-3} eV^{-1} this is accompanied by a steep band profile across the oxide that even exhibits a local maximum. Nevertheless, the measurable pinning offset is hardly influenced at all by this profile (cf. $D_0 = 1 \times 10^{19}$ cm^{-3} eV^{-1} and $D_0 = 1 \times 10^{19}$ cm^{-3} eV^{-1}).

3. Summary and Conclusions

We have quantified here a model that describes the universal energy alignment of organic molecules on oxide-covered metals, as recently demonstrated by Greiner et al.[29] without any adjustable parameters. It is based on three factors:

i) the Schottky–Mott rule of molecules weakly interacting with their substrate, and hence the absence of any interface dipoles on the atomic level that would affect the energy difference $\Phi_{sub} - IE_{org}$ as it is inferred from the corresponding quantities measured spectroscopically for the substrate and the organic molecules separately;
ii) the charge equilibrium between the electronic systems of the organic molecules and the underlying substrate as expressed by the Fermi–Dirac distribution function;
iii) the condition of overall charge neutrality.

In a first approximation, the oxide has the function of a dielectric and does not participate in the charge exchange. This implies that for situations where the frontier orbitals of the molecule (the only ones considered) are energetically sufficiently removed from the Fermi level, the charge exchange is negligible and the level alignment according to the Schottky–Mott regime holds. When the frontier orbitals approach the Fermi level, Fermi–Dirac statistics and the condition of charge neutrality require a charge exchange, which increases the closer the two are in energy. Simultaneously, a potential drop across the oxide realigns the Fermi level and the frontier orbitals of the molecules to counteract the charge transfer. Because the potential drop is itself determined by the amount of transferred charge and the capacitance of the metal oxide-molecule arrangement, the problem has to be solved self consistently. As we have shown, this leads to a pinning of the HOMO 0.14 eV below E_F, because the charge needed to ensure thermal equilibrium is on average far less than 1% for each molecule at densities in excess of one monolayer. Hence, the HOMO energy lies below the Fermi level in the steep tail of the Fermi–Dirac distribution function. An analogous scenario holds for equilibrium charge exchange between E_F and LUMO with the LUMO lying by the same amount above E_F.

On a second level of sophistication we consider the charge distribution and the ensuing potential drop within the organic layer. This is again done self consistently and leads to essentially the same result as before, albeit with a pinning position of the HOMO 0.33 eV below E_F for a layer thickness of 11 nm, a value that is in perfect agreement with the 0.33 ± 0.05 eV of Greiner et al.[29] At the same time, the calculations reproduce the "band bending" towards higher binding energy with a layer thickness that is widely observed experimentally.[17,29,35,36]

In a last step we have considered the effect of a finite density of defects in the oxide. Numerical calculations again confirm that neither the transition from the Schottky–Mott regime to the pinning regime nor the pinning position itself are measurably influenced by oxide defects up to a level where the density of states due to defects reaches 5×10^{19} eV^{-1} cm^{-3}. This is so despite the fact that charge transferred to the defect levels distorts the potential in the oxide significantly compared with the defect-free case.

Finally, on all levels of approximation, the pinning position shows only a weak logarithmic dependence on all system parameters, such as the thicknesses and permittivities of the oxide and organic layers, and the results including the pinning positions carry even over to a situation without oxide, provided integer charge transfer between the organic molecules and the substrate is the only factor responsible for energy alignment.

The universality and robustness of the pinning position, as observed by Greiner et al.[29] for small organic molecules, and by Salaneck's group[26] for polymers, rely on two factors. Firstly, the average amount of charge on each molecule is small for layers in excess of a monolayer. Molecules can carry at most one unit of charge on account of Coulomb repulsion, and yet far less than a monolayer of fully charged molecules right at the interface will fulfill the self-consistent charge-exchange condition and pin E_{HOMO}. Hence, for coverages of a few to many MLs, as were encountered in most of the experimental studies, there will be little further change in the level alignment.

This robustness is also reflected in the small scatter of ±0.05 eV in the ΔE_H values in the pinning regime, as seen in Figure 2b. This fact leads us to conclude that the much larger scatter of the data in the Schottky–Mott regime is not due to uncertainties in ΔE_H but rather due to variations in $\Phi_{sub} - IE_{org.}$ It is unlikely that the variations in $\Phi_{sub} - IE_{org}$ reflect experimental uncertainties, because both Φ_{sub} and IE_{org} were determined by the same technique as ΔE_H, namely photoelectron spectroscopy. Hence, there has to be a physical origin of the horizontal scatter in the data. While IE_{org} is experimentally accessible even after interface formation, $\Phi_{sub,interface}$ is not. Therefore, it is plausible that $\Phi_{sub,interface}$, as it determines the level alignment after interface formation, differs from Φ_{sub} as measured for the bare substrate. The obvious mechanism for such a modification is the formation of an interface dipole that changes the substrate's work function by an amount δ. Hence, $\Phi_{sub,interface} = \Phi_{sub} + \delta$ would have been the correct quantity to enter our model instead of Φ_{sub}. The difference between the data and our model calculation in the Schottky–Mott regime of Figure 5 in terms of $\Phi_{sub} - IE_{org}$ equals δ. There appears to be a systematic and a random deviation of the data points from the model curve. The systematic deviation amounts to $\langle\delta\rangle \approx 0.35$ eV which corresponds to an increase in $\Phi_{sub.}$ The random scatter of ±0.20 eV reflects

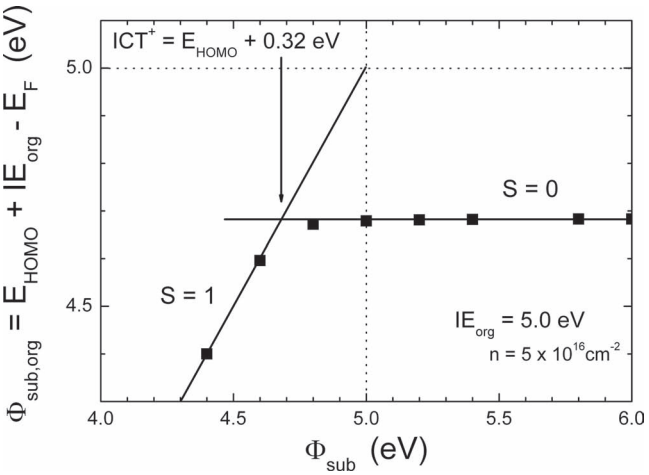

Figure 11. Full level alignment calculation (data points) plotted in the form of a "Zorro" diagram (cf. Figure 1) for a coverage of 5×10^{16} cm^{-2} organic molecules (≈8 nm thickness) with an ionization potential of 5.0 eV. For details see text.

the individual deviation of the particular oxide-molecule interface dipole from the average dipole. Widely discussed in the literature on organic interfaces and also introduced by Greiner et al.[29] is the so-called push-back effect. This effect refers to the push back of the electron spill-out from the substrate by the organic overlayer, which effectively decreases the substrate's work function (i.e., $\delta < 0$). This is opposite to the average $<\delta>$ and hence cannot be responsible for the deviation. For the class of interfaces discussed here, it therefore appears that the Schottky–Mott regime holds quantitatively with an uncertainty of ±0.20 eV after a correction of +0.35 eV has been applied to Φ_{sub}.

Our calculation has implications for the work of Salaneck, Fahlmann and co-workers as well.[13,14,26] In **Figure 11**, we present our model results near the intersection of the Schottky–Mott ($S = 1$) and the pinning regime ($S = 0$) in a form that corresponds to the "Zorro" diagram of Figure 1. To this end we assume a specific organic molecule with $IE_{org} = 5.0$ eV and replace the $\Phi_{sub} - IE_{org}$ abscissa by Φ_{sub}. From the HOMO position relative to E_F, the work function of the organic overlayer,

Table 1. Fermi level pinning positions of organic molecules on various substrates for cases of weak interaction.

Substrate/ Adlayer	Adlayer orbital energy (eV)		Authors	Reference
	$E_F - E_{HOMO}$	$E_{LUMO} - E_F$		
PEDOT:PSS/copper phthalocyanine (CuPc)	0.4		Peisert et al.	[37]
PEDOT:PSS/fluorinated copper phthalocyanine ($CuPcF_4$)	0.5		Peisert et al.	[37]
PEDOT:PSS/poly(9,9′-dioctylfluorene-*co*-bis-*N*,*N*′-(4-butylphenyl)-bis-*N*,*N*′-phenyl-1,4-phenylenediamine) (PFB)	0.44		Hwang et al.	[38]
ozoned Au/poly(9,9′-dioctylfluorene-*co*-bis-*N*,*N*′-(4-butylphenyl)-bis-*N*,*N*′-phenyl-1,4-phenylenediamine) (PFB)	0.45		Hwang et al.	[38]
PEDOT:PSS/poly(9,9′-dioctylfluorene) (F8)	0.49		Hwang et al.	[38]
PEDOT:PSS/poly(9,9′-dioctylfluorene) (F8)	0.36[a)]		Hwang et al.	[38]
PEDOT:PFESA/(N,N'-bis-(1-naphthyl)-N,N'-diphenyl1-1,1-biphenyl1-4,4-diamine) (NPB)	0.4		Braun et al.	[39]
Ca/copper phthalocyanine (CuPc)	0.4		Tanaka et al.	[40]
Mg/copper phthalocyanine (CuPc)	0.4		Tanaka et al.	[40]
Sm/copper phthalocyanine (CuPc)	0.4		Tanaka et al.	[40]
PEDOT:PFESA/poly(3-hexylthiophene) (P3HT)	0.5		Tengstedt et al.	[41]
PEDOT:PSS/poly(3-hexylthiophene) (P3HT)	0.5		Tengstedt et al.	[41]
indium tin oxide/poly(3-hexylthiophene) (P3HT)	0.5		Tengstedt et al.	[41]
Oxidized Silicon/poly(3-hexylthiophene) (P3HT)	0.5		Tengstedt et al.	[41]
PEDOT:PFESA/poly(9-(1′-decylundecylidene)fluorene) (P10AF)	0.4		Tengstedt et al.	[41]
PEDOT:PSS/poly(9-(1′-decylundecylidene)fluorene) (P10AF)	0.4		Tengstedt et al.	[41]
PEDOT:PFESA/poly(2,7-9,9-(di(oxy-2,5,8-trioxadecane))fluorene) (PFO)	0.6		Tengstedt et al.	[41]
PEDOT:PFESA/poly(2,7-9,9-(di(oxy-2,5,8-trioxadecane))fluorene) (PFO)	0.6		Tengstedt et al.	[41]
indium tin oxide/tetrafluorotetracyanoquinodimethane (F_4TCNQ)		0.3	Braun et al.	[39]
PEDOT-PSS/tetrafluorotetracyanoquinodimethane (F_4TCNQ)		0.3	Braun et al.	[39]
PEDOT-PFESA/tetrafluorotetracyanoquinodimethane (F_4TCNQ)		0.3	Braun et al.	[39]
Au/tetracyanoquinodimethane (TCNQ)		0.2	Murdey et al.	[42]
indium tin oxide/tetracyanoquinodimethane (TCNQ)		0.2	Murdey et al.	[42]
PEDOT-PSS/tetracyanoquinodimethane (TCNQ)		0.2	Murdey et al.	[42]
poly(9,9′-dioctylfluorene) (F8)/C_{60}		0.5	Osikowicz et al.	[14]

[a)]In the limit of one monolayer.

$\Phi_{sub,org}$, is obtained by adding IE_{org}, and this is the scale of the ordinate in Figure 11. The result of the simulation is represented by a series of individual points mimicking an experimental data set and to these are fitted two straight lines with slopes $S = 1$ and $S = 0$, respectively. In the spirit of Salaneck and co-workers,[26] the substrate work function at the intersection of the two lines is assigned to the energy of the ICT^+ relative to the vacuum level. The result, 4.68 eV turns out to lie 0.32 eV above E_{HOMO}. This difference would be interpreted by Salaneck and co-workers[26] as polaronic binding energy as discussed in the introduction. However, our model treats the spectroscopically determined HOMO as the charge-transfer state without any polaronic relaxation effects and yet yields the apparent polaronic binding energy of 0.32 eV. This demonstrates that a major fraction of the polaronic binding energy of 0.5 ± 0.1 eV, as reported by Salaneck and co-workers,[26] is in reality due to the fact that in equilibrium the position of the HOMO does not coincide with E_F, as implicitly assumed in the interpretation of the "Zorro" diagram by Salaneck and co-workers,[26] but lies 0.32 eV below E_F.

Finally, in **Table 1** we have collected the pinning positions of E_F relative to the HOMO of a wide range of organic molecule/substrate combinations where there is sometimes direct, more often circumstantial evidence that the interaction at the interface is weak. The central message is that in no case is E_F pinned right at E_{HOMO}. The same is true for the cases where a pinning of E_F near the LUMO is observed. In both cases, the difference between E_F and the transport orbital, and thus the injection barrier, for carriers is at least 0.3 eV, in excellent agreement with our calculation. This universal behavior reflects the fact that our results do not depend on the detailed aspects of the organic material, such as conformational degrees of freedom, growth mode, crystalline vs. amorphous films, etc., as long as the Schottky–Mott rule holds.

Acknowledgements

We are particularly indebted to M. Greiner who has supported our work with numerous explanations of his approach and by generously providing crucial additional information on his experiments. Without his help this note would not have been possible.

Received: May 25, 2012
Revised: August 2, 2012
Published online: October 1, 2012

[1] D. Braga, G. Horowitz, *Adv. Mater.* **2009**, *21*, 1473.
[2] V. Coropceanu, J. Cornil, D. A. da Silva, Y. Olivier, R. Silbey, J. L. Bredas, *Chem. Rev.* **2007**, *107*, 926.
[3] S. R. Forrest, *Org. Electron.* **2003**, *4*, 45.
[4] S. R. Forrest, *Nature* **2004**, *428*, 911.
[5] G. Horowitz, *Adv. Mater.* **1998**, *10*, 365.
[6] C. J. Brabec, N. S. Sariciftci, J. C. Hummelen, *Adv. Funct. Mater.* **2001**, *11*, 15.
[7] J. L. Bredas, J. E. Norton, J. Cornil, V. Coropceanu, *Acc. Chem. Res.* **2009**, *42*, 1691.
[8] P. Peumans, A. Yakimov, S. R. Forrest, *J. Appl. Phys.* **2003**, *93*, 3693.
[9] G. Yu, J. Gao, J. C. Hummelen, F. Wudl, A. J. Heeger, *Science* **1995**, *270*, 1789.
[10] D. Cahen, A. Kahn, *Adv. Mater.* **2003**, *15*, 271.
[11] I. G. Hill, D. Milliron, J. Schwartz, A. Kahn, *Appl. Surf. Sci.* **2000**, *166*, 354.
[12] H. Vazquez, W. Gao, F. Flores, A. Kahn, *Phys. Rev. B: Condens. Matter* **2005**, *71*, 4.
[13] X. Crispin, V. Geskin, A. Crispin, J. Cornil, R. Lazzaroni, W. R. Salaneck, J. L. Bredas, *J. Am. Chem. Soc.* **2002**, *124*, 8131.
[14] W. Osikowicz, M. P. de Jong, W. R. Salaneck, *Adv. Mater.* **2007**, *19*, 4213.
[15] S. Duhm, Q. Xin, S. Hosoumi, H. Fukagawa, K. Sato, N. Ueno, S. Kera, *Adv. Mater.* **2012**, *24*, 901.
[16] H. Fukagawa, S. Kera, T. Kataoka, S. Hosoumi, Y. Watanabe, K. Kudo, N. Ueno, *Adv. Mater.* **2007**, *19*, 665.
[17] H. Y. Mao, F. Bussolotti, D. C. Qi, R. Wang, S. Kera, N. Ueno, A. T. S. Wee, W. Chen, *Org. Electron.* **2011**, *12*, 534.
[18] T. Sueyoshi, H. Fukagawa, M. Ono, S. Kera, N. Ueno, *Appl. Phys. Lett.* **2009**, *95*, 183303.
[19] T. Sueyoshi, H. Kakuta, M. Ono, K. Sakamoto, S. Kera, N. Ueno, *Appl. Phys. Lett.* **2010**, *96*, 093303.
[20] S. Duhm, I. Salzmann, G. Heimel, M. Oehzelt, A. Haase, R. L. Johnson, J. P. Rabe, N. Koch, *Appl. Phys. Lett.* **2009**, *94*, 033304.
[21] J. Frisch, M. Schubert, E. Preis, J. P. Rabe, D. Neher, U. Scherf, N. Koch, *J. Mater. Chem.* **2012**, *22*, 4418.
[22] N. Koch, *J. Phys.: Condens. Matter* **2008**, *20*, 12.
[23] I. Salzmann, S. Duhm, R. Opitz, R. L. Johnson, J. P. Rabe, N. Koch, *J. Appl. Phys.* **2008**, *104*, 11.
[24] I. Salzmann, G. Heimel, S. Duhm, M. Oehzelt, P. Pingel, B. M. George, A. Schnegg, K. Lips, R. P. Blum, A. Vollmer, N. Koch, *Phys. Rev. Lett.* **2012**, *108*, 5.
[25] D. Steinmuller, M. G. Ramsey, F. P. Netzer, *Phys. Rev. B: Condens. Matter* **1993**, *47*, 13323.
[26] S. Braun, W. R. Salaneck, M. Fahlman, *Adv. Mater.* **2009**, *21*, 1450.
[27] J. Hwang, A. Wan, A. Kahn, *Mater. Sci. Eng. R: Rep.* **2009**, *64*, 1.
[28] W. Mönch, *Semiconductor Surfaces and Interfaces*, Springer-Verlag, Berlin, **1995**.
[29] M. T. Greiner, M. G. Helander, W. M. Tang, Z. B. Wang, J. Qiu, Z. H. Lu, *Nat. Mater.* **2012**, *11*, 76.
[30] M. T. Edmonds, M. Wanke, A. Tadich, H. M. Vulling, K. J. Rietwyk, P. L. Sharp, C. B. Stark, Y. Smets, A. Schenk, Q. H. Wu, L. Ley, C. I. Pakes, *J. Chem. Phys.* **2012**, *136*, 9.
[31] J. E. Field, *The Properties of Natural and Synthetic Diamond*, Academic Press, London, **1992**.
[32] S. H. Lo, D. A. Buchanan, Y. Taur, W. Wang, *IEEE Electron. Device Lett.* **1997**, *18*, 209.
[33] N. F. Mott, E. A. Davis, *Electronic Processes in Non-Crystalline Materials*, Clarendon Press, Oxford, **1979**.
[34] H. Fritzsche, M. Cuevas, *Phys. Rev.* **1960**, *119*, 1238.
[35] H. Ishii, N. Hayashi, E. Ito, Y. Washizu, K. Sugi, Y. Kimura, M. Niwano, Y. Ouchi, K. Seki, *Phys. Status Solidi A* **2004**, *201*, 1075.
[36] H. Ishii, K. Sugiyama, E. Ito, K. Seki, *Adv. Mater.* **1999**, *11*, 605.
[37] H. Peisert, A. Petr, L. Dunsch, T. Chasse, M. Knupfer, *ChemPhysChem* **2007**, *8*, 386.
[38] J. Hwang, E. G. Kim, J. Liu, J. L. Bredas, A. Duggal, A. Kahn, *J. Phys. Chem. C* **2007**, *111*, 1378.
[39] S. Braun, W. R. Salaneck, *Chem. Phys. Lett.* **2007**, *438*, 259.
[40] Y. Tanaka, K. Kanai, Y. Ouchi, K. Seki, *Org. Electron.* **2009**, *10*, 990.
[41] C. Tengstedt, W. Osikowicz, W. R. Salaneck, I. D. Parker, C. H. Hsu, M. Fahlman, *Appl. Phys. Lett.* **2006**, *88*, 053502.
[42] R. J. Murdey, W. R. Salaneck, *Jpn. J. Appl. Phys., Part 1* **2005**, *44*, 3751.